Devito (v3.1.0): an embedded domain-specific language for finite differences and geophysical exploration

Mathias Louboutin[1], Michael Lange[2], Fabio Luporini[3], Navjot Kukreja[3], Philipp A. Witte[1], Felix J. Herrmann[1], Paulius Velesko[3], and Gerard J. Gorman[3]

[1]School of Computational Science and Engineering, Georgia Institute of Technology, Atlanta, USA
[2]ECMWF, UK
[3]Earth Science and Engineering, Imperial College London, London, UK

Correspondence to: Mathias Louboutin (mlouboutin3@gatech.edu)

Abstract.

We introduce Devito, a new domain-specific language for implementing high-performance finite difference partial differential equation solvers. The motivating application is exploration seismology where methods such as Full-Waveform Inversion and Reverse-Time Migration are used to invert terabytes of seismic data to create images of the earth's subsurface. Even using
5   modern supercomputers, it can take weeks to process a single seismic survey and create a useful subsurface image. The computational cost is dominated by the numerical solution of wave equations and their corresponding adjoints. Therefore, a great deal of effort is invested in aggressively optimizing the performance of these wave-equation propagators for different computer architectures. Additionally, the actual set of partial differential equations being solved and their numerical discretization is under constant innovation as increasingly realistic representations of the physics are developed, further ratcheting up the cost
10   of practical solvers. By embedding a domain-specific language within Python and making heavy use of SymPy, a symbolic mathematics library, we make it possible to develop finite difference simulators quickly using a syntax that strongly resembles the mathematics. The Devito compiler reads this code and applies a wide range of analysis to generate highly optimized and parallel code. This approach can reduce the development time of a verified and optimized solver from months to days.

1   Introduction

15   Large-scale inversion problems in exploration seismology constitute some of the most computationally demanding problems in industrial and academic research. Developing computationally efficient solutions for applications such as seismic inversion requires expertise ranging from theoretical and numerical methods for partial differential equation (PDE) constrained optimization to low-level performance optimization of PDE solvers. Progress in this area is often limited by the complexity and cost of developing bespoke wave propagators (and their discrete adjoints) for each new inversion algorithm or formulation of wave
20   physics. Traditional software engineering approaches often lead developers to make critical choices regarding the numerical discretization before manual performance optimization for a specific target architecture and making it ready for production. This workflow of bringing new algorithms into production, or even to a stage that they can be evaluated on realistic datasets can take many person-months or even person-years. Furthermore, it leads to mathematical software that is not easily ported,

maintained or extended. In contrast, the use of high-level abstractions and symbolic reasoning provided by domain-specific languages (DSL) can significantly reduce the time it takes to implement and verify individual operators for use in inversion frameworks, as has already been shown for the finite element method (Logg et al., 2012; Rathgeber et al., 2015; Farrell et al., 2013).

5 State-of-the-art seismic imaging is primarily based upon explicit finite difference schemes due to their relative simplicity and ease of implementation (Virieux, 1986; Symes, 2015a; Weiss and Shragge, 2013). When considering how to design a DSL for explicit finite difference schemes, it is useful to recognize the algorithm as being primarily a sub-class of stencil algorithms or polyhedral computation (Henretty et al., 2013; Andreolli et al., 2015; Yount, 2015). However, stencil compilers lack two significant features required to develop a DSL for finite differences: symbolic computational support required to express finite

10 difference discretizations at a high level, enabling these expressions to be composed and manipulated algorithmically; support for algorithms that are not stencil-like, such as source and receiver terms that are both sparse and unaligned with the finite difference grid. Therefore, the design aims behind the Devito DSL can be summarized as:

– create a high-level mathematical abstraction for programming finite differences to enable composability and algorithmic optimization,

15 – insofar as possible use existing compiler technologies to optimize the affine loop nests of the computation, which account for most of the computational cost,

– develop specific extensions for other parts of the computation that are non-affine (e.g., source and receiver terms).

The first of these aims is primarily accomplished by embedding the DSL in *Python* and leveraging the symbolic mathematics package Sympy (Meurer et al., 2017). From this starting point, an abstract syntax tree is generated and standard compiler

20 algorithms can be employed to either generate optimized and parallel C code or to write code for a stencil DSL - which itself will be passed to the next compiler in the chain. The fact that this can be all performed just-in-time (JIT) means that a combination of static and dynamic analysis can be used to generate optimized code. However, in some circumstances, one might also choose to compile offline.

The use of symbolic manipulation, code generation and just-in-time compilation allows the definition of individual wave

25 propagators for inversion in only a few lines of *Python* code, while aspects such as varying the problem discretization become as simple as changing a single parameter in the problem specification, for example changing the order of the spatial discretization Louboutin et al. (2017). This article explains *what* can be accomplished with Devito, showing how to express real-life wave propagators as well as their integration within larger workflows typical of seismic exploration, such as the popular Full-Waveform Inverison (FWI) and Reverse-Time Migration (RTM) methods. The Devito compiler, and in particular

30 *how* the user-provided SymPy equations are translated into high-performance C, are also briefly summarized, although for a complete description the interested reader should refer to Luporini et al. (2018).

The remainder of this paper is structured as follows: first, we provide a brief history of optimizing compilers, DSL and existing wave equation seismic frameworks. Next, we highlight the core features of Devito and describe the implementation of

the featured wave equation operators in Section 3. We outline the seismic inversion theory in Section 4. Code verification and analysis of accuracy in Section 5 is followed by a discussion of the propagators computational performance in Section 6. We conclude by presenting a set of realistic seismic inversion examples and a discussion of future work.

2 Background

5   Improving the runtime performance of a critical piece of code on a particular computing platform is a non-trivial task that has received significant attention throughout the history of computing. The desire to automate the performance optimization process itself across a range of target architectures is not new either, although it is often met with skepticism. Even the very first compiler, A0 Hopper (1952), was received with resistance, as best summarized in the following quote: *"Dr. Hopper believes,..., that the result of a compiling technique should be a routine just as efficient as a hand tailored routine. Some others*

10   *do not completely agree with this. They feel the machine-made routine can approach hand tailored coding, but they believe there are "tricks of the trade" that apply to various special cases that a computer cannot be expected to utilize."* (Jones, 1954). Given the challenges of porting optimized codes to a wide range of rapidly evolving computer architectures, it seems natural to raise again the layer of abstraction and use compiler techniques to replace much of the manual labor.

  Community acceptance of these new "automatic coding systems" began when concerns about the performance of the gen-

15   erated code were addressed by the first "optimizing compiler", FORTRAN, released in 1957 – which not only translated code from one language to another but also ensured that the final code performed at least as good as a hand-written low-level code (Backus, 1978). Since then, as program and hardware complexity rose, the same problem has been solved over and over again, each time by the introduction of higher levels of abstractions. The first high-level languages and compilers were targeted at solving a large variety of problems and hence were restricted in the kind of optimizations they could leverage.

20   As these generic languages became common-place and the need for further improvement in performance was felt, restricted languages focusing on smaller problem domains were developed that could leverage more "tricks of the trade" to optimize performance. This led to the proliferation of DSLs for broad mathematical domains or sub-domains, such as APL (Iverson, 1962), Mathematica, Matlab®or R.

  In addition to these relatively general mathematical languages, more specialized frameworks targeting the automated solution

25   of PDEs have long been of interest (Cárdenas and Karplus, 1970; Umetani, 1985; Cook Jr, 1988; Van Engelen et al., 1996). More recent examples not only aim to encapsulate the high-level notation of PDEs, but are often centered around a particular numerical method. Two prominent contemporary projects based on the finite element method (FEM), FEniCS (Logg et al., 2012) and Firedrake (Rathgeber et al., 2015), both implement a common DSL, UFL (Alnæs et al., 2014), that allows the expression of variational problems in weak form. Multiple DSLs to express stencil-like algorithms have also emerged over

30   time, including Henretty et al. (2013); Zhang and Mueller (2012); Christen et al. (2011); Unat et al. (2011); Köster et al. (2014); Membarth et al. (2012); Osuna et al. (2014); Tang et al. (2011); Bondhugula et al. (2008); Yount (2015). Other stencil DSLs have been developed with the objective of solving PDEs using finite differences Hawick and Playne (2013), Arbona et al. (2017) and Jacobs et al. (2016). However, in all cases their use in seismic imaging problems (or even more broadly in

science and engineering) has been limited by a number of factors other than technology inertia. Firstly, they only raise the abstraction to the level of polyhedral-like (affine) loops. As they do not generally use a symbolic mathematics engine to write the mathematical expressions at a high-level, developers must still write potentially complex numerical kernels in the target low-level programming language. For complex formulations this process can be time consuming and error prone, as hand-
5   tuned codes for wave propagators can reach thousands of lines of code. Secondly, most DSLs rarely offer enough flexibility for extension beyond their original scope (e.g. sparse operators for source terms and interpolation) making it difficult to work the DSL into a more complex science/engineering workflow. Finally, since finite difference wave propagators only form part of the over-arching PDE constrained (wave equation) optimization problem, composability with external packages, such as the *SciPy* optimization toolbox, is a key requirement that is often ignored by self-contained standalone DSLs. The use of a fully
10   embedded *Python* DSL, on the other hand, allows users to leverage a variety of higher-level optimization techniques through a rich variety of software packages provided by the scientific *Python* ecosystem.

Moreover, several computational frameworks for seismic imaging exist, although they provide varying degrees of abstraction and are typically limited to a single representation of the wave equation. IWAVE (Symes et al., 2011; Symes, 2015b; Sun and Symes, 2010; Symes, 2015a), although not a DSL, provides a high-level of abstraction and a mathematical framework
15   to abstract the algebra related to the wave-equation and its solution. IWAVE provides a rigorous mathematical abstraction for linear operations and vector representations including Hilbert space abstraction for norms and distances. However, its C++ implementation limits the extensibility of the framework to new wave-equations. Other software frameworks, such as Madagascar (Fomel et. al, 2013), offer a broad range of applications. Madagascar is based on a set of subroutines for each individual problem and offers modelling and imaging operators for multiple wave-equations. However, the lack of high-level
20   abstraction restricts its flexibility and interfacing with high level external software (i.e *Python* , *Java*). The subroutines are also mostly written in C/Fortran and limit the architecture portability.

3   Symbolic definition of finite difference stencils with Devito

In general, the majority of the computational workload in wave-equation based seismic inversion algorithms arises from computing solutions to discrete wave equations and their adjoints. There are a wide range of mathematical models used in seismic
25   imaging that approximate the physics to varying degrees of fidelity. To improve development and innovation time, including code verification, we describe the use of the symbolic finite difference framework Devito to create a set of explicit matrix-free operators of arbitrary spatial discretization order. These operators are derived for example from the acoustic wave equation

$$m(x)\frac{\partial^2 u(t,x)}{\partial t^2} - \Delta u(t,x) = q(t,x), \tag{1}$$

where $m(x) = \frac{1}{c(x)^2}$ is the squared slowness with $c(x)$ the spatially dependent speed of sound, symbol $\Delta u(t,x)$ denotes the
30   Laplacian of the wavefield $u(t,x)$ and $q(t,x)$ is a source usually located at a single location x_s in space ($q(t,x) = f(t)\delta(x_s)$). This formulation will be used as running example throughout the section.
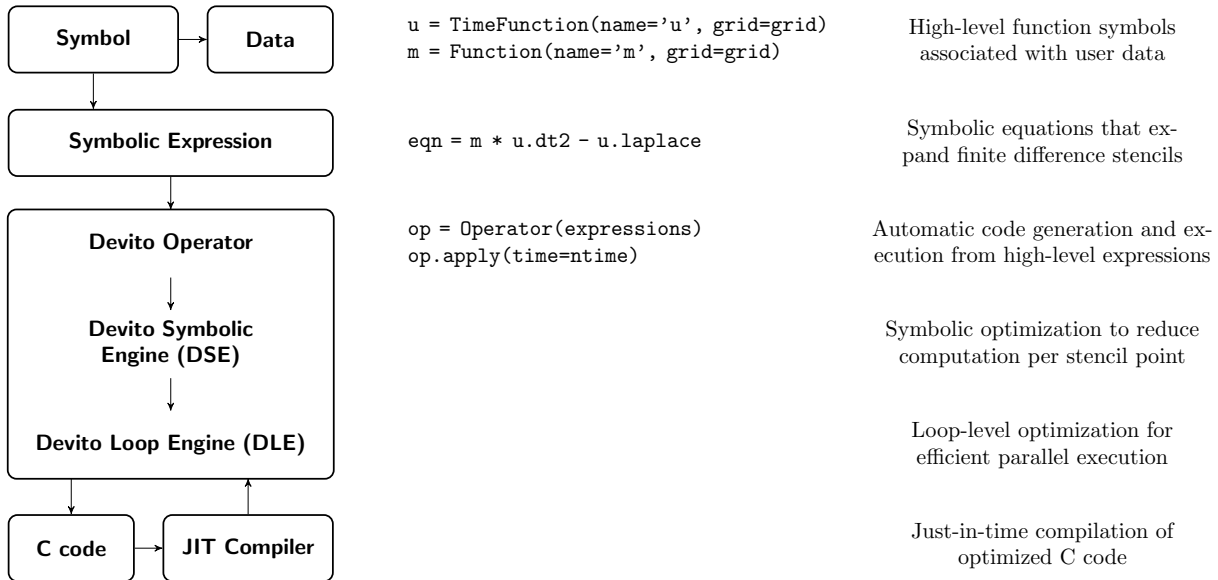
Figure 1. Overview of the Devito architecture and the associated example workflow. Devito's top-level API allows users to generate symbolic stencil expressions using data-carrying function objects that can be used to for symbolic expressions via *SymPy* . From this high-level definition an operator then generates, compiles and executes high-performance C code.

3.1 Code generation - an overview

Devito aims to combine performance benefits of dedicated stencil frameworks (Bondhugula et al., 2008; Tang et al., 2011; Henretty et al., 2013; Yount, 2015) with the expressiveness of symbolic PDE-solving DSLs (Logg et al., 2012; Rathgeber et al., 2015) through automated code generation and optimization from high-level symbolic expressions of the mathematics.

5 Thus, the primary design objectives of the Devito DSL are to allow users to define explicit finite difference operators for (time-dependent) PDEs in a concise symbolic manner, and provide an API that is flexible enough to fully support realistic scientific use cases. To this end, Devito offers a set of symbolic classes that are fully compatible with the general-purpose symbolic algebra package *SymPy* that enables users to derive discretized stencil expressions in symbolic form. As we show in Fig. 1, the primary symbols in such expressions are associated with user data that carry domain-specific meta-data information to be used

10 by the compiler engine (e.g. dimensions, data type, grid). The discretized expressions form an abstract operator definition that Devito uses to generate low-level C code (C99) and OpenMP at runtime. The encapsulating `Operator` object can be used to execute the generated code from within the *Python* interpreter making Devito natively compatible with the wide range of tools available in the scientific *Python* software stack.

A Devito `Operator` takes as input a collection of symbolic expressions and progressively lowers the symbolic representa-
15 tion to semantically equivalent C code. The code generation process consists of a sequence of compiler passes during which multiple automated performance-optimization techniques are employed. These can be broadly categorised into two classes and are performed by distinct sub-packages:

– **Devito Symbolic Engine (DSE):** Symbolic optimization techniques, such as Common Sub-expression Elimination (CSE), factorization and loop-invariant code motion are utilized to reduce the number of floating point operations (flops) performed within the computational kernel (Luporini et al., 2015).

– **Devito Loop Engine (DLE):** Well-known loop optimization techniques, such as explicit vectorization, thread-level parallelization and loop blocking with auto-tuned block sizes are employed to increase the cache utilization and thus memory bandwidth utilization of the kernels.

A complete description of the compilation pipeline is provided in Luporini et al. (2018).

3.2 Discrete function symbols

The primary user-facing API of Devito allows the definition of complex stencil operators from a concise mathematical notation. For this purpose Devito relies strongly on *SymPy* . Devito provides two symbolic object types that mimic *SymPy* symbols, enabling the construction of stencil expressions in symbolic form:

– **Function:** The primary class of symbols provided by Devito behaves like `sympy.Function` objects, allowing symbolic differentiation via finite difference discretization and general symbolic manipulation through *SymPy* utilities. Symbolic function objects encapsulate state variables (parameters and solution of the PDE) in the operator definition and associated user data (function value) with the represented symbol. The meta-data, such as grid information and numerical type, which provide domain-specific information to the Devito compiler are also carried by the `sympy.Function` object.

– **Dimension:** Each `sympy.Function` object defines an iteration space for stencil operations through a set of `Dimension` objects that are used to define and generate the corresponding loop structure from the symbolic expressions.

In addition to `sympy.Function` and `Dimension` symbols, Devito supplies the construct `Grid`, which encapsulates the definition of the computational domain and defines the discrete shape (number of grid points, grid spacing) of the function data. The number of spatial dimensions are hereby derived from the shape of the `Grid` object and inherited by all `Function` objects, allowing the same symbolic operator definitions to be used for two and three-dimensional problem definitions. As an example, a two-dimensional discrete representation of the square slowness of an acoustic wave $m[x,y]$ inside a 5 by 6 grid points domain can be created as a symbolic function object as illustrated in Fig. 2.

It is important to note here that $m[x,y]$ is constant in time, while the discrete wavefield $u[t,x,y]$ is time-dependent. Since time is often used as the stepping dimension for buffered stencil operators, Devito provides an additional function type `TimeFunction`, which automatically adds a special `TimeDimension` object to the list of dimensions. As an example, we can create an equivalent symbolic representation of the wavefield as `u = TimeFunction(name='u', grid=grid)`, which is denoted symbolically as `u(t, x, y)`.

```
>>> grid = Grid(shape=(5, 6))
>>> m = Function(name='m', grid=grid)

>>> m
m(x, y)

>>> m.data.shape
(5, 6)
```

Figure 2. Defining a Devito `Function` on a `Grid`

3.2.1 Spatial discretization

The symbolic nature of the function objects allows the automatic derivation of discretized finite difference expressions for derivatives. Devito `Function` objects provide a set of shorthand notations that allow users to express, for example, $\frac{d\boldsymbol{u}[t,x,y,z]}{dx}$ as `u.dx` and $\frac{d^2\boldsymbol{u}[t,x,y,z]}{dx^2}$ as `u.dx2`. Moreover, the discrete Laplacian, defined in three dimensions as $\Delta\boldsymbol{u}[t,x,y,z] = \frac{d^2\boldsymbol{u}[t,x,y,z]}{dx^2} + \frac{d^2\boldsymbol{u}[t,x,y,z]}{dy^2} + \frac{d^2\boldsymbol{u}[t,x,y,z]}{dz^2}$ can be expressed in shorthand simply as `u.laplace`. The shorthand expression `u.laplace` is agnostic to the number of spatial dimensions and may be used for two or three-dimensional problems.

The discretization of the spatial derivatives can be defined for any order. In the most general case, we can write the spatial discretization in the x direction of order k (and equivalently in the y and z direction) as:

$$\frac{\partial^2\boldsymbol{u}[t,x,y,z]}{\partial x^2} = \frac{1}{h_x^2}\sum_{j=1}^{\frac{k}{2}}\left[\alpha_j(\boldsymbol{u}[t,x+jh_x,y,z] + \boldsymbol{u}[t,x-jh_x,y,z])\right], \tag{2}$$

where h_x is the discrete grid spacing in dimension x, the constants α_j are the coefficients of the finite difference scheme and the spatial discretization error is of order $O(h_x^k)$.

3.2.2 Temporal discretization

We consider here a second-order time discretization for the acoustic wave equation, as higher order time discretization requires us to rewrite the PDE (Seongjai Kim, 2007). The discrete second-order time derivative with this scheme can be derived from the Taylor expansion of the discrete wavefield $\boldsymbol{u}(t,x,y,z)$ as

$$\frac{d^2\boldsymbol{u}[t,x,y,z]}{dt^2} = \frac{\boldsymbol{u}[t+\Delta t,x,y,z] - 2\boldsymbol{u}[t,x,y,z] + \boldsymbol{u}[t-\Delta t,x,y,z]}{\Delta t^2}. \tag{3}$$

In this expression, Δt is the size of a discrete time step. The discretization error is $O(\Delta t^2)$ (second order in time) and will be verified in Section. 5.

Following the convention used for spatial derivatives, the above expression can be automatically generated using the shorthand expression `u.dt2`. Combining the temporal and spatial derivative notations, and ignoring the source term q, we can now define the wave propagation component of Equation 1 as a symbolic expression via `Eq(m * u.dt2 - u.laplace,`

```
>>> from sympy import Eq, solve, init_printing, pprint
>>> init_printing(use_latex=True)
>>> from devito import Function, TimeFunction, Grid

>>> grid = Grid(shape=(5, 5))
>>> u = TimeFunction(name='u', grid=grid, space_order=2, time_order=2)
>>> m = Function(name='m',grid=grid)

>>> eqn = Eq(m * u.dt2 - u.laplace)
>>> stencil = solve(eqn, u.forward)[0]
>>> pprint(Eq(u.forward, stencil))
```

Produces output equivalent to:

$$
\begin{aligned}
u(t+s,x,y) = 2u(t,x,y) - u(t-s,x,y) \\
\left. \begin{aligned}
- \frac{2s^2 u(t,x,y)}{h_y^2 m(x,y)} + \frac{s^2 u(t,x,y-h_y)}{h_y^2 m(x,y)} + \frac{s^2 u(t,x,y+h_y)}{h_y^2 m(x,y)} \\
- \frac{2s^2 u(t,x,y)}{h_x^2 m(x,y)} + \frac{s^2 u(t,x-h_x,y)}{h_x^2 m(x,y)} + \frac{s^2 u(t,x+h_x,y)}{h_x^2 m(x,y)}
\end{aligned} \right\} \frac{\Delta t^2 \Delta u}{m(x,y)}
\end{aligned}
$$

Figure 3. Example code defining the two-dimensional wave equation without damping using Devito symbols and symbolic processing utilities from *SymPy*. Assuming $h_x = \Delta x$, $h_y = \Delta y$ and $s = \Delta t$ the output is equivalent to Eq. 1 without the source term $\boldsymbol{q}_s$.

0) where Eq is the *SymPy* representation of an equation. In the resulting expression all spatial and temporal derivatives are expanded using the corresponding finite difference terms. To define the propagation of the wave in time, we can now rearrange the expression to derive a stencil expression for the forward stencil point in time, $\boldsymbol{u}(t+\Delta t,x,y,z)$, denoted by the shorthand expression u.forward. The forward stencil corresponds to the explicit Euler time-stepping that updates the next

5 time-step u.forward from the two previous ones u and u.backward (Equation. 4). We use the *SymPy* utility solve to automatically derive the explicit time-stepping scheme, as shown in Figure 3 for a second order in space discretization.

$$
\boldsymbol{u}[t+\Delta t,x,y,z] = 2\boldsymbol{u}[t,x,y,z] - \boldsymbol{u}[t-\Delta t,x,y,z] + \frac{\Delta t^2}{\boldsymbol{m}[x,y,z]} \Delta \boldsymbol{u}[t,x,y,z]. \tag{4}
$$

The iteration over time to obtain the full solution is then generated by the Devito compiler from the time dimension information. Solving the wave-equation with the above explicit Euler scheme is equivalent to a linear system $\mathbf{A}(\boldsymbol{m})\boldsymbol{u} = \boldsymbol{q}_s$ where

10 the vector $\boldsymbol{u}$ is the discrete wavefield solution of the discrete wave-equation, $\boldsymbol{q}_s$ is the source term and $\mathbf{A}(\boldsymbol{m})$ is the matrix representation of the discrete wave-equation. From Eq. 4 we can see that the matrix $\mathbf{A}(\boldsymbol{m})$ is a lower triangular matrix that reflects the time-marching structure of the stencil. Simulation of the wavefield is equivalent to a forward substitution (solve row by row from the top) on the lower triangular matrix $\mathbf{A}(\boldsymbol{m})$. Since we do not consider complex valued PDEs, the adjoint of $\mathbf{A}(\boldsymbol{m})$ is equivalent to its transpose denoted as $\mathbf{A}^\top(\boldsymbol{m})$ and is an upper triangular matrix. The solution $\boldsymbol{v}$ of the discrete

15 adjoint wave-equation $\mathbf{A}(\boldsymbol{m})^\top \boldsymbol{v} = \boldsymbol{q}_a$ for an adjoint source $\boldsymbol{q}_a$ is equivalent to a backward substitution (solve from bottom row

to top row) on the upper triangular matrix $\mathbf{A}(\boldsymbol{m})^{\top}$ and is simulated backward in time starting from the last time-step. These matrices are never explicitly formed, but are instead matrix free operators with implicit implementation of the matrix-vector product, $\boldsymbol{u} = \mathbf{A}(\boldsymbol{m})^{-1}\boldsymbol{q}_s$ as a forward stencil. The stencil for the adjoint wave-equation in this self-adjoint case would simply be obtained with `solve(eqn, u.backward)` and the compiler will detect the backward-in-time update.

3.2.3 Boundary conditions

The field recorded data is measured on a wavefield that propagates in an infinite domain. However, solving the wave equation in a discrete infinite domain is not feasible with finite differences. In order to mimic an infinite domain, Absorbing Boundary Conditions (ABC) or Perfectly Matched Layers (PML) are necessary (Clayton and Engquist, 1977). These two methods allow the approximation of the wavefield as it is in an infinite medium by damping and absorbing the waves within an extra layer at the limit of the domain to avoid unnatural reflections from the edge of the discrete domain.

The least computationally expensive method is the Absorbing Boundary Conditions that adds a single damping mask in a finite layer around the physical domain. This absorbing condition can be included in the wave-equation as

$$\boldsymbol{m}[x,y,z]\frac{d^2\boldsymbol{u}[t,x,y,z]}{dt^2} - \Delta\boldsymbol{u}[t,x,y,z] + \boldsymbol{\eta}[x,y,z]\frac{d\boldsymbol{u}[t,x,y,z]}{dt} = 0. \tag{5}$$

The $\boldsymbol{\eta}[x,y,z]$ parameter is equal to 0 inside the physical domain and increasing from inside to outside within the damping layer. The dampening parameter $\boldsymbol{\eta}$ can follow a linear or exponential curve depending on the frequency band and width of the dampening layer. For methods based on more accurate modelling, for example in simulation-based acquisition design (Liu and Fomel, 2011; Wason et al., 2017; Naghizadeh and Sacchi, 2009; Kumar et al., 2015), a full implementation of the PML will be necessary to avoid weak reflections from the domain limits.

3.2.4 Sparse point interpolation

Seismic inversion relies on data fitting algorithms, hence we need to support sparse operations such as source injection and wavefield ($\boldsymbol{u}[t,x,y,z]$) measurement at arbitrary grid locations. Both operations occur at sparse domain points, which do not necessarily align with the logical cartesian grid used to compute the discrete solution $\boldsymbol{u}(t,x,y,z)$. Since such operations are not captured by the finite differences abstractions for implementing PDEs, Devito implements a secondary high-level representation of sparse objects (Lange et al., 2017) to create a set of *SymPy* expressions that perform polynomial interpolation within the containing grid cell from pre-defined coefficient matrices.

The necessary expressions to perform interpolation and injection are automatically generated through a dedicated symbol type, `SparseFunction`, which associates a set of coordinates with the symbol representing a set of non-aligned points. For examples, the syntax `p.interpolate(expr)` provided by a `SparseFunction` `p` will generate a symbolic expressions that interpolates a generic expression `expr` onto the sparse point locations defined by `p`, while `p.inject(field, expr)` will evaluate and add `expr` to each enclosing point in `field`. The generated *SymPy* expressions are passed to Devito `Operator` objects alongside the main stencil expression to be incorporated into the generated C kernel code. A complete

setup of the acoustic wave equation with absorbing boundaries, injection of a source function and measurement of wavefields via interpolation at receiver locations can be found in Section 4.2.

4 Seismic modeling and inversion

Seismic inversion methods aim to reconstruct physical parameters or an image of the earth's subsurface from multi-experiment field measurements. For this purpose a wave is generated at the ocean surface that propagates through to the subsurface and creates reflections at the discontinuities of the medium. The reflected and transmitted waves are then captured by a set of hydrophones that can be classified as either moving receivers (cables dragged behind a source vessel) or static receivers (ocean bottom nodes or cables). From the acquired data, physical properties of the subsurface such as wave speed or density can be reconstructed by minimizing the misfit between the recorded measurements and the numerically modelled seismic data.

4.1 Full-Waveform Inversion

Recovering the wave speed of the subsurface from surface seismic measurements is commonly cast into a non-linear optimization problem called full-waveform inversion (FWI). The method aims at recovering an accurate model of the discrete wave velocity, c, or alternatively the square slowness of the wave, $m = \frac{1}{c^2}$ (not an overload), from a given set of measurements of the pressure wavefield u. Lions (1971); Tarantola (1984); Virieux and Operto (2009); Haber et al. (2012) shows that this can be expressed as a PDE-constrained optimization problem. After elimination of the PDE constraint, the reduced objective function is defined as:

$$\underset{\boldsymbol{m}}{\text{minimize}} \quad \Phi_s(\boldsymbol{m}) = \frac{1}{2} \|\mathbf{P}_r \boldsymbol{u} - \boldsymbol{d}\|_2^2 \quad \text{with:} \quad \boldsymbol{u} = \mathbf{A}(\boldsymbol{m})^{-1} \mathbf{P}_s^T \boldsymbol{q}_s, \tag{6}$$

where $\mathbf{P}_r$ is the sampling operator at the receiver locations, $\mathbf{P}_s^T$ (^{T} is the transpose or adjoint) is the injection operator at the source locations, $\mathbf{A}(\boldsymbol{m})$ is the operator representing the discretized wave equation matrix, $\boldsymbol{u}$ is the discrete synthetic pressure wavefield, $\boldsymbol{q}_s$ is the corresponding pressure source and $\boldsymbol{d}$ is the measured data. While we consider the acoustic isotropic wave equation for simplicity here, in practice, multiple implementations of the wave equation operator $\boldsymbol{A}(\boldsymbol{m})$ are possible depending on the choice of physics. In the most advanced case, $\boldsymbol{m}$ would not only contain the square slowness but also anisotropic or orthorhombic parameters.

To solve this optimization problem with a gradient-based method, we use the adjoint-state method to evaluate the gradient (Plessix, 2006; Haber et al., 2012):

$$\nabla \Phi_s(\boldsymbol{m}) = \sum_{\boldsymbol{t}=1}^{n_t} \boldsymbol{u}[\boldsymbol{t}] \boldsymbol{v}_{tt}[\boldsymbol{t}] = \mathbf{J}^T \delta \boldsymbol{d}_s, \tag{7}$$

where n_t is the number of computational time steps, $\delta \boldsymbol{d}_s = (\mathbf{P}_r \boldsymbol{u} - \boldsymbol{d})$ is the data residual (difference between the measured data and the modeled data), $\mathbf{J}$ is the Jacobian operator and $\boldsymbol{v}_{tt}$ is the second-order time derivative of the adjoint wavefield that solves:

$$\mathbf{A}^T(\boldsymbol{m})\boldsymbol{v} = \mathbf{P}_r^T \delta \boldsymbol{d}. \tag{8}$$

The discretized adjoint system in Eq. 8 represents an upper triangular matrix that is solvable by modelling wave propagation backwards in time (starting from the last time step). The adjoint state method, therefore, requires a wave equation solve for both the forward and adjoint wavefields to compute the gradient. An accurate and consistent adjoint model for the solution of
5   the optimization problem is therefore of fundamental importance.

4.2 Acoustic forward modelling operator

We consider the acoustic isotropic wave-equation for a squared slowness $\boldsymbol{m}[x,y,z]$. We have zero initial conditions assuming the wavefield does not have any energy before zero time. We have an additional dampening term to mimic an infinite domain (see sec 3.2.3). We have zero Dirichlet boundary conditions as the solution is considered to be fully damped at the limit of the
10   computational domain. The PDE is defined in Eq. 5. Figure 4 demonstrates the complete set up of the acoustic wave equation with absorbing boundaries, injection of a source function and sampling wavefields at receiver locations. The shape of the computational domain is hereby provided by a utility object `model`, while the damping term $\eta \frac{d\boldsymbol{u}[x,y,z,t]}{dt}$ is implemented via a utility symbol `eta` defined as a `Function` object. It is important to note that the discretization order of the spatial derivatives is passed as an external parameter `order` and carried as meta-data by the wavefield symbol `u` during construction, allowing
15   the user to freely change the underlying stencil order.

The main (PDE) stencil expression to update the state of the wavefield is derived from the high-level wave equation expression `eqn = u.dt2 - u.laplace + damp*u.dt` using *SymPy* utilities as demonstrated before in Fig. 3. Additional expressions for the injection of the wave source via the `SparseFunction` object `src` are then generated for the forward wavefield, where the source time signature is discretized onto the computational grid via the symbolic expression `src *`
20   `dt**2 / m`. The weight $\frac{dt^2}{m}$ is derived from rearranging the discretized wave equation with a source as a right-hand-side similarly to the Laplacian in Eq. 4. A similar expression to interpolate the current state of the wavefield at the receiver locations (measurement points) is generated through the `receiver` symbol. The combined list of stencils, a sum in Python that adds the different expressions that update the wavefield at the next time step, inject the source and interpolate at the receivers, is then passed to the `Operator` constructor alongside a definition of the spatial and temporal spacing $h_x, h_y, h_z, \Delta t$ provided
25   by the `model` utility. Devito then transforms this list of stencil expressions into loops (inferred from the symbolic Functions), replaces all necessary constants by their values if requested, prints the generated C code and compiles it. The operator is finally callable in Python with `op.apply()`.

4.3 Discrete adjoint wave-equation and FWI gradient

To create the adjoint that pairs with the above forward modeling propagator we can make use of the fact that the isotropic
30   acoustic wave equation is self-adjoint. This entails that for the implementation of the forward wave equation `eqn`, shown in Fig. 5, only the sign of the damping term needs to be inverted, as the dampening time-derivative has to be defined in the

```
def forward(model, source, receiver, space_order=2):
    m, eta = model.m, model.damp
    # Allocate wavefield and auxiliary fields
    u = TimeFunction(name='u', grid=model.grid, time_order=2,
                     space_order=space_order)

    # Derive stencil from symbolic equation
    eqn = m * u.dt2 - u.laplace + eta * u.dt
    stencil = solve(eqn, u.forward)
    update_u = Eq(u.forward, stencil)

    # Source injection and receiver interpolation
    src = source.inject(field=u.forward, expr=src * dt**2 / m)
    rec = receiver.interpolate(expr=u)

    op = Operator([update_u] + src + rec, subs=model.spacing_map)
```

Figure 4. Example definition of a forward operator.

```
def adjoint(model, adj_src, adj_rec, space_order=2):
    m, eta = model.m, model.damp
    # Allocate wavefield and auxiliary fields
    v = TimeFunction(name='v', grid=model.grid,
                     time_order=2, space_order=space_order)

    # Derive stencil from symbolic equation
    eqn = m * v.dt2 - v.laplace - eta * v.dt
    stencil = solve(eqn, v.backward)
    update_v = Eq(u.backward, stencil)

    # Receiver injection and adj-source interpolation
    src_a = adj_src.inject(field=v.backward,
                           expr=rec * dt**2 / m)
    rec_a = adj_rec.interpolate(expr=v)

    op = Operator([update_v] + src_a + rec_a,
                  subs=model.spacing_map)
```

Figure 5. Example definition of an adjoint operator.

```
def gradient(model, u, adj_src, space_order=2):
    m, eta = model.m, model.damp
    # Allocate wavefield and auxiliary fields
    v = TimeFunction(name='v', grid=model.grid,
                     time_order=2, space_order=space_order)
    grad = Function(name='grad', grid=model.grid)

    # Derive stencil from symbolic equation
    eqn = m * v.dt2 - v.laplace - eta * v.dt
    stencil = solve(eqn, v.backward)
    update_v = Eq(u.backward, stencil)

    # Receiver injection and gradient update
    src_a = adj_src.inject(field=v.backward,
                           expr=rec * dt**2 / m)
    update_grad = Eq(grad, grad - u * v.dt2)

    op = Operator([update_v] + src_a + update_grad,
                  subs=model.spacing)
```

Figure 6. Example definition of a gradient operator.

direction of propagation ($\frac{\partial}{\partial n(t)}$). For the PDE stencil, however, we now rearrange the stencil expression to update the backward wavefield from the two next time steps as $\boldsymbol{v}[t - \Delta t, x, y, z] = f(\boldsymbol{v}[t, x, y, z], \boldsymbol{v}[t + \Delta t, x, y, z])$. Moreover, the role of the sparse point symbols has changed (Eq. 8), so that we now inject time-dependent data at the receiver locations (`adj_src`), while sampling the wavefield at the original source location (`adj_rec`).

Based on the definition of the adjoint operator, we can now define a similar operator to update the gradient according to Eq. 7. As shown in Fig. 6, we can replace the expression to sample the wavefield at the original source location with an accumulative update of the gradient field `grad` via the symbolic expression `Eq(grad, grad - u * v.dt2)`.

To compute the gradient, the forward wavefield at each time step must be available which leads to significant memory requirements. Many methods exist to tackle this memory issue, but all come with their advantages and disadvantages. For instance, we implemented optimal checkpointing based on its library Revolve in Devito to drastically reduce the memory cost by only saving a partial time history and recomputing the forward wavefield when needed (Kukreja et al., 2018). The

5 memory reduction comes at an extra computational cost as optimal checkpointing requires $log(n_t)+2$ extra PDE solves. Another method is boundary wavefield reconstruction (McMechan, 1983; Mittet, 1994; Raknes and Weibull, 2016) that saves the wavefield only at the boundary of the model, but still requires us to recompute the forward wavefield during the back-propagation. This boundary method has a reduced memory cost but necessitates the computation of the forward wavefield twice (one extra PDE solve), once to get the data than a second time from the boundary values to compute the gradient.

10 **4.4 FWI using Devito operators**

At this point we have a forward propagator to model synthetic data in Fig. 4, the adjoint propagator for Eq 8 and the FWI gradient of Eq. 7 in Fig. 6. With these three operators, we show the implementation of the FWI objective and gradient with Devito in Fig. 8. With the forward and adjoint/gradient operator defined for a given source, we only need to add a loop over all the source experiments and the reduction operation on the gradients (sum the gradient for each source experiment

15 together). In practice, this loop over sources is where the main task-based or MPI based parallelization happens. The wave-equation propagator does use some parallelization with multithreading or domain decomposition but that parallelism requires communication. The parallelism over source experiment is task-based and does not require any communication between the separate tasks as the gradient for each source can be computed independently and reduced to obtain the full gradient. With the complete gradient summed over the source experiments, we update the model with a simple fixed step length gradient update

20 (Cauchy, 1847).

This FWI function in Fig. 7 can then be included in any black-box optimization toolbox such as *SciPy* `optimize` to solve the inversion problem Eq.6. While black-box optimization methods aim to minimize the objective, there are no guarantees they find a global minimum because the objective is highly non-linear in m and other more sophisticated methods are required (Warner and Guasch, 2014; van Leeuwen and Herrmann, 2015; Peters and Herrmann, 2017; Witte et al., 2018).

25 **5 Verification**

Given the operators defined in Section 3 we now verify the correctness of the code generated by the Devito compiler. We first verify that the discretized wave equation satisfies the convergence properties defined by the order of discretization, and secondly we verify the correctness of the discrete adjoint and computed gradient.

```python
def fwi_gradient(model, op_fwd, op_grad):
    """
    Function to compute a single FWI gradient
    """
    u = TimeFunction(name='u', grid=model.grid,
                     space_order=order)
    grad = Function(name='grad', grid=model.grid)

    for i in nshots:
        # Update source location for each shot
        src.coordinates.data[0. :] = source_loc[i]

        # Run forward modelling operator
        op_fwd(u=u, src=src, rec=smooth_d)

        # Compute gradient from data residual and
        # update objective function
        residual = smooth_d.data[:] - true_d.data[:]
        objective += .5*np.linalg.norm(residual)**2
        op_grad(rec=residual, u=u, m=model.m, grad=grad)

    return objective, grad.data
```

Figure 7. Definition of FWI gradient update.

```python
model = Model(...)
dt, nt = <timestepping parameters>

# Define source and receiver geometry
src = RickerSource(...)
rec = Receiver(...)

# Create forward and gradient operators
op_fwd = forward(model, src, rec, order)
op_grad = gradient(model, rec, order)

# Run FWI with gradient descent
for i in range(0, fwi_iterations):
    # Compute functional value and gradient
    # for the current model estimate
    phi, direction = fwi_gradient(model.m)

    # Artificial Step length for gradient descent
    alpha = .005 / np.max(direction)

    # Update the model estimate and inforce
    # minimum/maximum values
    m_updated = model.m.data - alpha*direction
    model.m.data[:] = box_constraint(m_updated)
```

Figure 8. FWI algorithm with linesearch.

5.1 Numerical accuracy

The numerical accuracy of the forward modeling operator (Fig. 4) and the runtime achieved for a given spatial discretization order and grid size are compared to the analytical solution of the wave equation in a constant media. We define two measures of the accuracy that compare the numerical wavefield in a constant velocity media to the analytical solution:

5   – **Accuracy versus size**, where we compare the obtained numerical accuracy as a function of the spatial sampling size (grid spacing).

   – **Accuracy versus time**, where we compare the obtained numerical accuracy as a function of runtime for a given physical model (fixed shape in physical units, variable grid spacing).

The measure of accuracy of a numerical solution relies on a hypothesis that we satisfy for these two tests:

10   – The domain is large enough and the propagation time small enough to ignore boundary related effects, i.e. the wavefield never reaches the limits of the domain.

   – The source is located on the grid and is a discrete approximation of the Dirac to avoid spatial interpolation errors. This hypothesis guarantees the existence of the analytical and numerical solution for any spatial discretization (Igel, 2016).
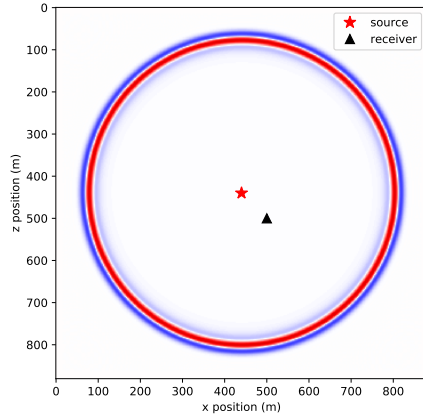
Figure 9. Numerical wavefield for a constant velocity $dt = .1$ms, $h = 1$m.
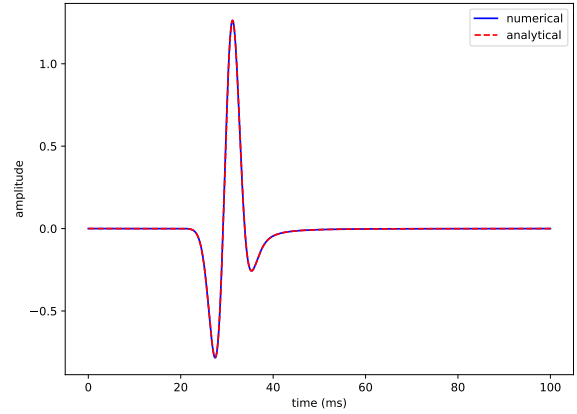
Figure 10. Numerical solution against analytical solution.

5.1.1 Convergence in time

We analyze the numerical solution against the analytical solution and verify that the error between these two decreases at a second order rate as a function of the time step size Δt. The velocity model is a $400\text{m} \times 400\text{m}$ domain with a source at the center. We compare the numerical solution to the analytical solution on Fig. 9, 10.

5   The analytical solution is defined as (Watanabe, 2015):

$$u_s(r,t) = \frac{1}{2\pi} \int\limits_{-\infty}^{\infty} \left\{ -i\pi H_0^{(2)}(kr) q(\omega) e^{i\omega t} d\omega \right\} \tag{9}$$

$$r = \sqrt{(x - x_{src})^2 + (y - y_{src})^2}, \tag{10}$$

where $H_0^{(2)}$ is the Hankel function of second kind and $q(\omega)$ is the spectrum of the source function. As we can see on Fig. 11 the error decreases near quadratically with the size of the time step with a time convergence rate of slope of 1.94 in logarithmic

10   scale that matches the theoretical expectation from a second order temporal discretization.

5.1.2 Spatial discretization analysis

The spatial discretization analysis follows the same method as the temporal discretixzation analysis. We model a wavefield for a fixed temporal setup with a small enough time-step to ensure negligeable time discretization error ($dt = .00625ms$). We vary the grid spacing (dx) and spatial discretization order and the and compute the error between the numerical and analytical

15   solution. The convergence rates should follow the theoretical rates defined in Eq. 2. In details, for a kth order discretization in space, the error between the numerical and analytical solution should decrease as $O(dx^k)$. The best way to look at the
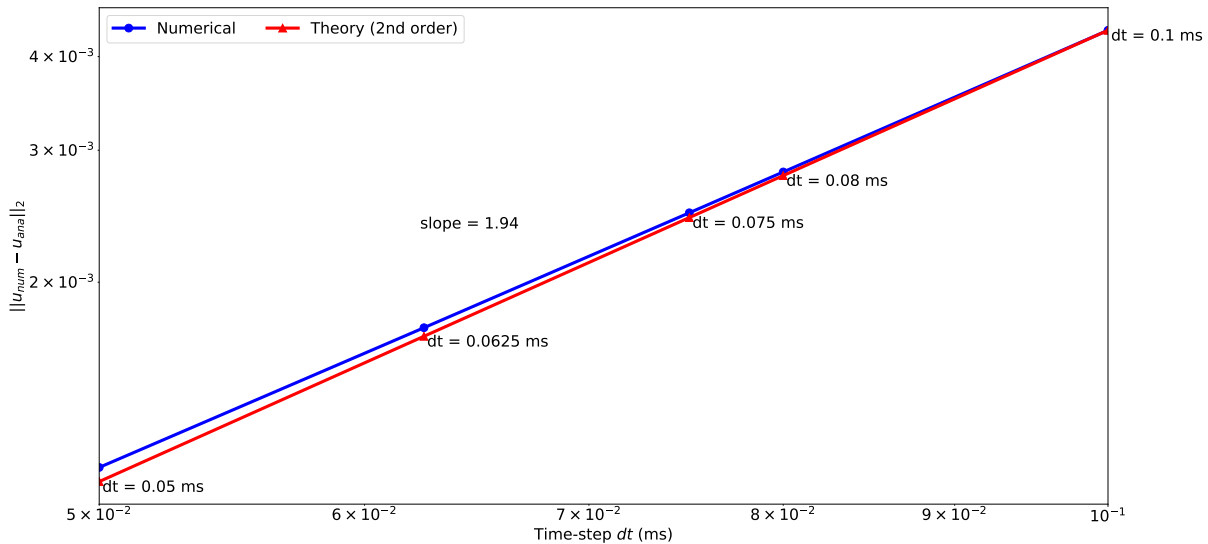
Figure 11. Time discretization convergence analysis for a fixed grid, fixed propagation time (150ms) and varying time step values. The result is plotted in a logarithmic scale and the numerical convergence rate (1.94 slope) shows that the numerical solution is accurate.

convergence results is yo plot the error in logarithmic scale and verify that the error decrease linearly with slope k. We show the converegence results on Fig. 12. The numerical convergence rates follow the theoretical ones for every tested order $k = 2, 4, 6, 8$ with the exception of the $10th$ order for small grid size. This is mainly due to reaching the limits of the numerical accuracy and a value of the error on par with the temporal discretization error. This behavior for high order and small grids is however in accordance with the literature as in in Wang et al. (2017).

The numerical slopes obtained and displayed on Fig. 12 demonstrate that the spatial finite difference follows the theoretical errors and converges to the analytical solution at the expected rate. These two convergence results (time and space) verify the accuracy and correctness of the symbolic discretization with Devito. With this validated simulated wavefield, we can now verify the implementation of the operators for inversion.

5.2 Propagators verification for inversion

We concentrate now on two tests, namely the adjoint test (or dot test) and the gradient test. The adjoint state gradient of the objective function defined in Eq. 7 relies on the solutions of the forward and adjoint wave equations, therefore, the first mandatory property to verify is the exact derivation of the discrete adjoint wave equation. The mathematical test we use is the standard adjoint property or dot-test:
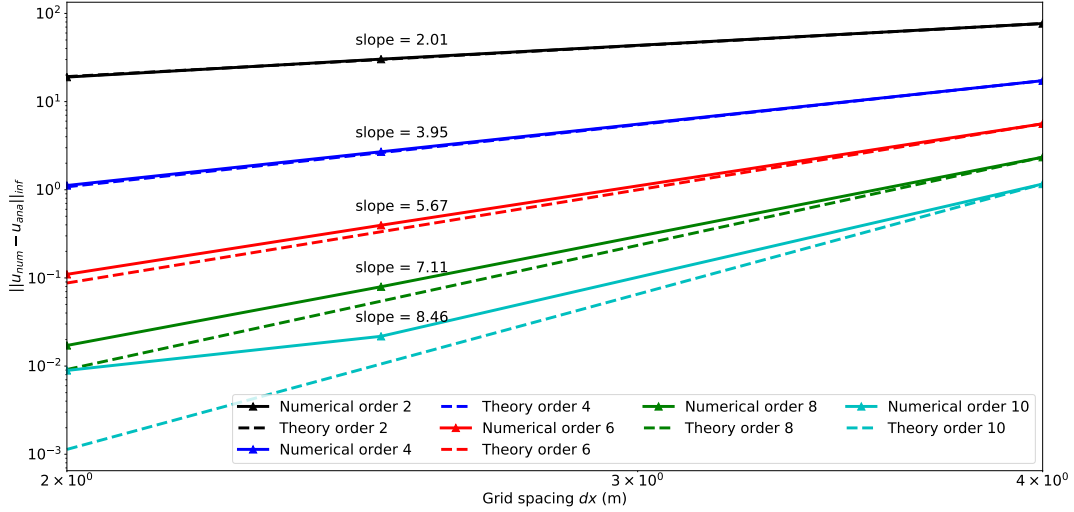
Figure 12. Comparison of the numerical convergence rate of the spatial finite difference scheme with the theoretical convergence rate from the Taylor theory. The theoretical rates are the dotted line with the corresponding colors. The result is plotted in a logarithmic scale to highlight the convergence orders as linear slopes and the numerical convergence rates show that numerical solution is accurate.

for any random $\boldsymbol{x} \in \text{span}(\boldsymbol{P}_s \boldsymbol{A}(\boldsymbol{m})^{-T} \boldsymbol{P}_r^{-T}), \boldsymbol{y} \in \text{span}(\boldsymbol{P}_r \boldsymbol{A}(\boldsymbol{m})^{-1} \boldsymbol{P}_s^{-T})$

$$\frac{< \boldsymbol{P}_r \boldsymbol{A}(\boldsymbol{m})^{-1} \boldsymbol{P}_s^{-T} \boldsymbol{x}, \boldsymbol{y} > - < \boldsymbol{x}, \boldsymbol{P}_s \boldsymbol{A}(\boldsymbol{m})^{-T} \boldsymbol{P}_r^{-T} \boldsymbol{y} >}{< \boldsymbol{P}_r \boldsymbol{A}(\boldsymbol{m})^{-1} \boldsymbol{P}_s^{-T} \boldsymbol{x}, \boldsymbol{y} >} = 0.0, \tag{11}$$

The adjoint test is also individually performed on the source/receiver injection/interpolation operators in the Devito tests suite. The results, summarized in Tables 1 and 2 with $\mathbf{F} = \boldsymbol{P}_r \boldsymbol{A}(\boldsymbol{m})^{-1} \boldsymbol{P}_s^{-T}$, verify the correct implementation of the adjoint operator for any order in both 2D and 3D. We observe that the discrete adjoint is accurate up to numerical precision for any order in 2D and 3D with an error of order $1e-16$. In combination with the previous numerical analysis of the forward modeling propagator that guarantees that we solve the wave equation, this result verifies that we the adjoint propagator is the exact numerical adjoint of the forward propagator and that it implements the adjoint wave equation.

With the forward and adjoint propagators tested, we finally verify that the Devito operator that implements the gradient of the FWI objective function (Eq. 7, Fig.6) is accurate with respect to the Taylor expansion of the FWI objective function. For a given velocity model and associated squared slowness $\boldsymbol{m}$, the Taylor expansion of the FWI objective function from Eq. 6 for a model perturbation $\boldsymbol{dm}$ and a perturbation scale h is:

$$\Phi_s(\boldsymbol{m} + h\boldsymbol{dm}) = \Phi_s(\boldsymbol{m}) + \mathcal{O}(h)$$
$$\Phi_s(\boldsymbol{m} + h\boldsymbol{dm}) = \Phi_s(\boldsymbol{m}) + h\langle \nabla \Phi_s(\boldsymbol{m}), \boldsymbol{dm} \rangle + \mathcal{O}(h^2). \tag{12}$$

Order	$<\mathbf{F}\boldsymbol{x}, \boldsymbol{y}>$	$<\boldsymbol{x}, \mathbf{F}^T\boldsymbol{y}>$	relative error
2nd order	7.9858e+05	7.9858e+05	0.0000e+00
4th order	7.3044e+05	7.3044e+05	0.0000e+00
6th order	7.2190e+05	7.2190e+05	4.8379e-16
8th order	7.1960e+05	7.1960e+05	4.8534e-16
10th order	7.1860e+05	7.1860e+05	3.2401e-16
12th order	7.1804e+05	7.1804e+05	6.4852e-16

Table 1. Adjoint test for different discretization orders in 2D, computed on a two layer model in double precision.

Order	$<\mathbf{F}\boldsymbol{x}, \boldsymbol{y}>$	$<\boldsymbol{x}, \mathbf{F}^T\boldsymbol{y}>$	relative error
2nd order	5.3840e+04	5.3840e+04	1.3514e-16
4th order	4.4725e+04	4.4725e+04	3.2536e-16
6th order	4.3097e+04	4.3097e+04	3.3766e-16
8th order	4.2529e+04	4.2529e+04	3.4216e-16
10th order	4.2254e+04	4.2254e+04	0.0000e+00
12th order	4.2094e+04	4.2094e+04	1.7285e-16

Table 2. Adjoint test for different discretization orders in 3D, computed on a two layer model in double precision.

These two equations constitute the gradient test where we define a small model perturbation $\boldsymbol{dm}$ and vary the value of h between 10^{-6} and 10^{0} and compute the error terms:

$$\epsilon_0 = \Phi_s(\boldsymbol{m} + h\boldsymbol{dm}) - \Phi_s(\boldsymbol{m})$$
$$\epsilon_1 = \Phi_s(\boldsymbol{m} + h\boldsymbol{dm}) - \Phi_s(\boldsymbol{m}) - h\langle\nabla\Phi_s(\boldsymbol{m}), \boldsymbol{dm}\rangle. \qquad (13)$$

We plot the evolution of the error terms as a function of the perturbation scale h knowing ϵ_0 should be first order (linear with slope 1 in a logarithmic scale) and ϵ_1 should be second order (linear with slope 2 in a logarithmic scale). We executed the gradient test defined in Eq. 12 in double precision with a 8th order spatial discretization. The test can be run for higher orders in the same manner but since it has already been demonstrated that the adjoint is accurate for all orders, the same results would be obtained.

In Fig. 13, the matching slope of the error term with the theoretical h and h^2 slopes from the Taylor expansion verifies the accuracy of the inversion operators. With all the individual parts necessary for seismic inversion, we now validate our implementation on a simple but realistic example.

5.3 Validation: Full-Waveform Inversion

We finally show a simple example of full-waveform inversion (FWI, Eq 7) on the Marmousi-ii model (Versteeg, 1994). This result obtained with the Julia interface to Devito JULI (Witte et al., 2018; Witte et al., 2018) that provides high-level abstraction for optimization and linear algebra. The model size is $4\mathrm{km} \times 16\mathrm{km}$ discretized with a $10\mathrm{m}$ grid in both directions. We use a $10\mathrm{Hz}$ Ricker wavelet with $4\mathrm{s}$ recording. The receivers are placed at the ocean bottom ($210\mathrm{m}$ depth) every $10\mathrm{m}$. We invert for the velocity with all the sources, spaced by $50\mathrm{m}$ at $10\mathrm{m}$ depth for a total of 300 sources. The inversion algorithm used is minConf_PQN(Schmidt et al., 2009), an l-BFGS algorithm with bounds constraints (minimum and maximum velocity values constraints). The result is shown in Fig. 14 and we can see that we obtain a good reconstruction of the true model. More advanced algorithms and constraints will be necessary for more complex problem such as less accurate initial model, noisy data or field recorded data (Witte et al., 2018; Peters and Herrmann, 2017); however the PDE solve part would not be impacted, making this example a good proof of concept for Devito.
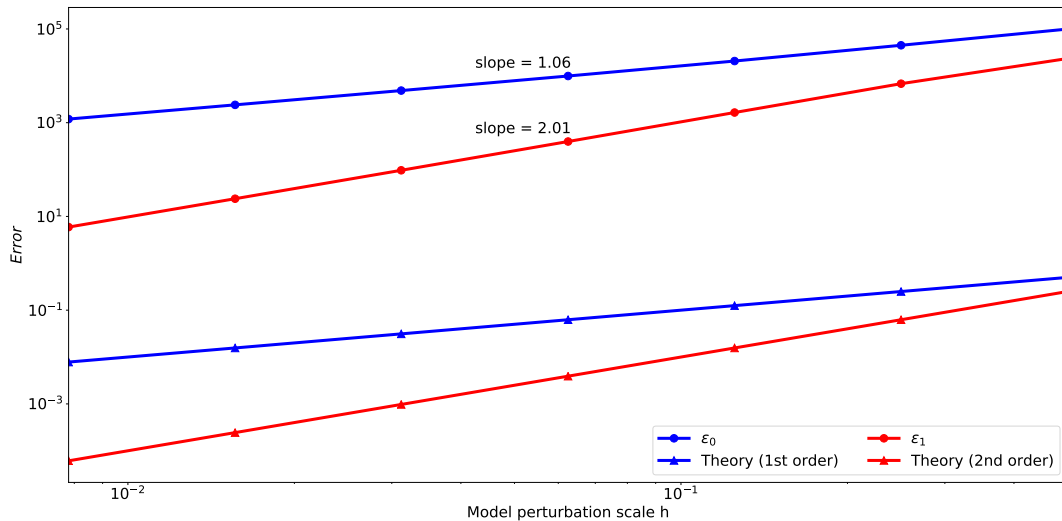
Figure 13. Gradient test for the acoustic propagator. The first order (blue) and second order (red) errors are displayed in logarithmic scales to highlight the slopes. The numerical convergence order (1.06 and 2.01) show that we have a correct implementation of the FWI operators.

This result highlights two main contributions of Devito. First, we provide PDE simulation tools that allow easy and efficient implementation of inversion operator for seismic problem and potentially any PDE constrained optimization problem. As described in Sec. 3 and 4, we can implement all the required propagators and the FWI gradient in a few lines in a concise and mathematical manner. Second, as we obtained this results with JUDI (Witte et al., 2018), a seismic inversion framework that provides a high-level linear abstraction layer on top of Devito for seismic inversion, this example illustrates that Devito is fully compatible with external languages and optimizations toolboxes and allows users to use our symbolic DSL for finite difference within their own inversion framework.

6 Performance

In this section we demonstrate the performance of Devito from the numerical and the inversion point of view, as well as the absolute performance from the hardware point of view. This section only provides a brief overview of Devito's performance and a more detailed description of the compiler and its performance is covered in Luporini et al. (2018).

6.1 Error-cost analysis

Devito's automatic code generation lets users define the spatial and temporal order of FD stencils symbolically and without having to reimplement long stencils by hand. This allows users to experiment with trade-offs between discretization errors and runtime, as higher order FD stencils provide more accurate solutions that come at increased runtime. For our error-cost analysis, we compare absolute error in L_2-norm between the numerical and the reference solution to the time-to-solution (the
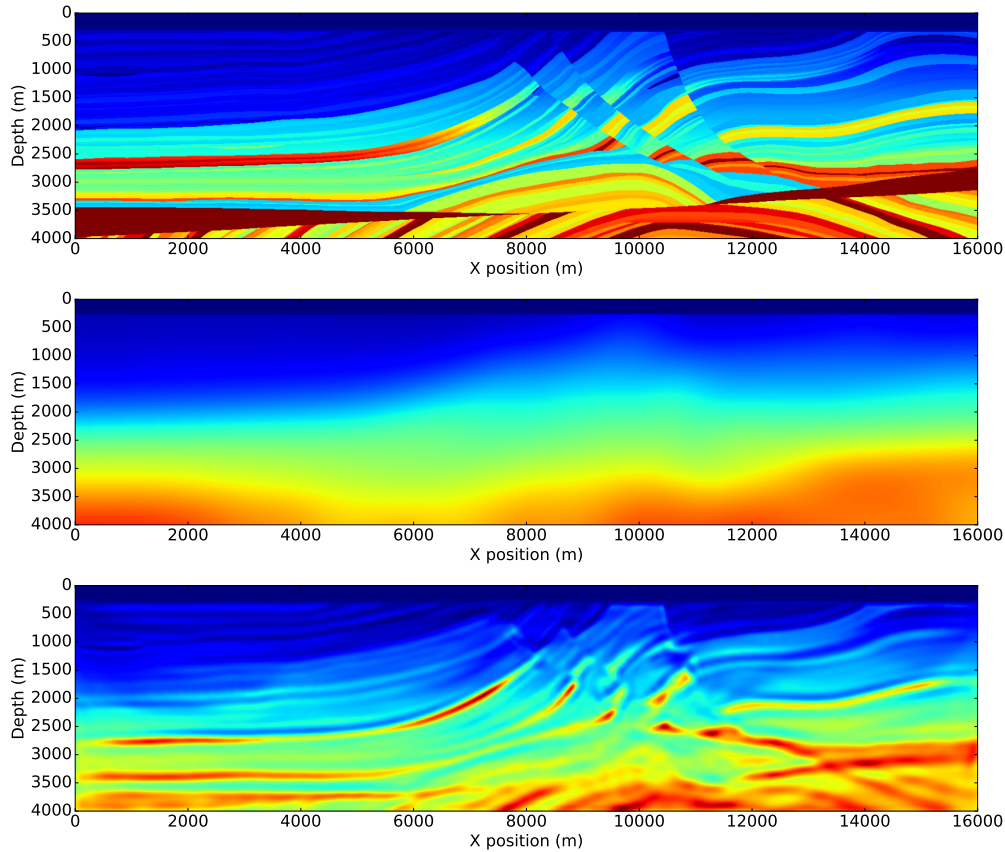
Figure 14. FWI on the acoustic Marmousi-ii model. The top plot is the true velocity model, the middle plot is the initial velocity model and the bottom one is the inverted velocity at the last iteration of the iterative inversion.

numerical and reference solution are defined in the previous Section 5). Figure 15 shows the runtime and numerical error obtained for a fixed physical setup. We use the same parameter as in Sec. 5.1 with a domain of $400\text{m} \times 400\text{m}$ and we simulate the wave propagation for 150ms.

The results in Fig. 15 illustrate that higher order discretizations produce a more accurate solution on a coarser grid with a

5   smaller runtime. This result is very useful for inverse problems, as a coarser grid requires less memory and fewer time steps. A grid size two times bigger implies a reduction of memory usage by a factor of 2^4 for 3D modeling. Devito then allows users to design FD simulators for inversion in an optimal way, where the discretization order and grid size can be chosen according to the desired numerical accuracy and availability of computational resources. The order of the FD stencils also affects the best possible hardware usage that can theoretically be achieved and whether an algorithm is compute or memory bound, a trade-off

10   that is described by the roofline model.
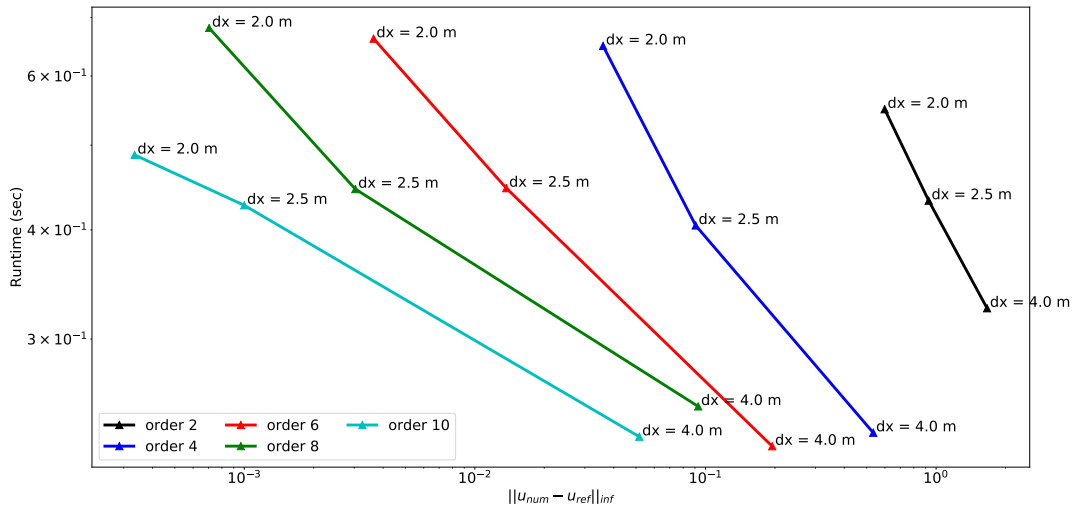
Figure 15. Different spatial discretization orders accuracy against runtime for a fixed physical setup (model size in m and propagation time).

6.2 Roofline analysis

We present performance results of our solver using the roofline model, as previously discussed in Colella (2004); Asanovic et al. (2006); Patterson and Hennessy (2007); Williams et al. (2009); Louboutin et al. (2017). Given a finite difference scheme, this method provides an estimate of the best achievable performance on the underlying architecture, as well as an

5 absolute measure of the hardware usage. We also show a more classical metric, namely *time to solution*, in addition to the roofline plots, as both are essential for a clear picture of the achieved performance. The experiments were run on an Intel Skylake 8180 architecture (28 physical cores, 38.5 MB shared L3 cache, with cores operating at 2.5 Ghz). The observed Stream TRIAD (McCalpin, 1991-2007) was 105 GB/s. The maximum single-precision FLOP performance was calculated as #cores · #avx units · #data items per vector register · 2(fused multiply-add) · core frequency = 4480 GFLOPs/s. A (more re-

10 alistic) performance peak of 3285 GFLOPs/s was determined by running the LINPACK benchmark (Dongarra, 1988). These values are used to construct the roofline plots.

We show three different roofline plots, one plot for each domain size attempted, in Fig. 16, 17 and 18. Different space orders are represented as different data points. The time-to-solution in seconds is annotated next to each data point. The experiments were run with all performance optimizations enabled. Because auto-tuning is used at runtime to determine the optimal loop-

15 blocking structure, timing only commences after autotuning has finished. The reported operational intensity benefits from the use of expression transformations as described in Section refsec:devito; particularly relevant for this problem is the factorization of FD weights.

We observe that the time to solution increases nearly linearly with the size of the domain. For example, for a 16th order discretization, we have a 17.1sec runtime for a $512 \times 512 \times 512$ domain and 162.6sec runtime for a $1024 \times 1024 \times 1024$

20 domain (8 times bigger domain and about 9 times slower). This is not surprising: the computation lies in the memory-bound
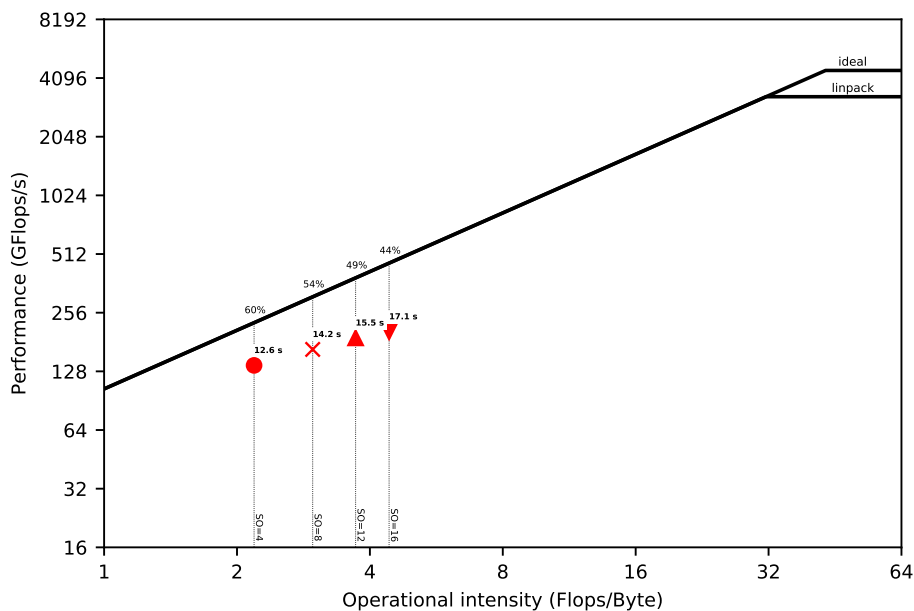
Figure 16. Roofline plots for a $512 \times 512 \times 512$ model on a Skylake 8180 architecture. The run times correspond to 1000ms of modeling for four different spatial discretization orders (4, 8, 12, 16).
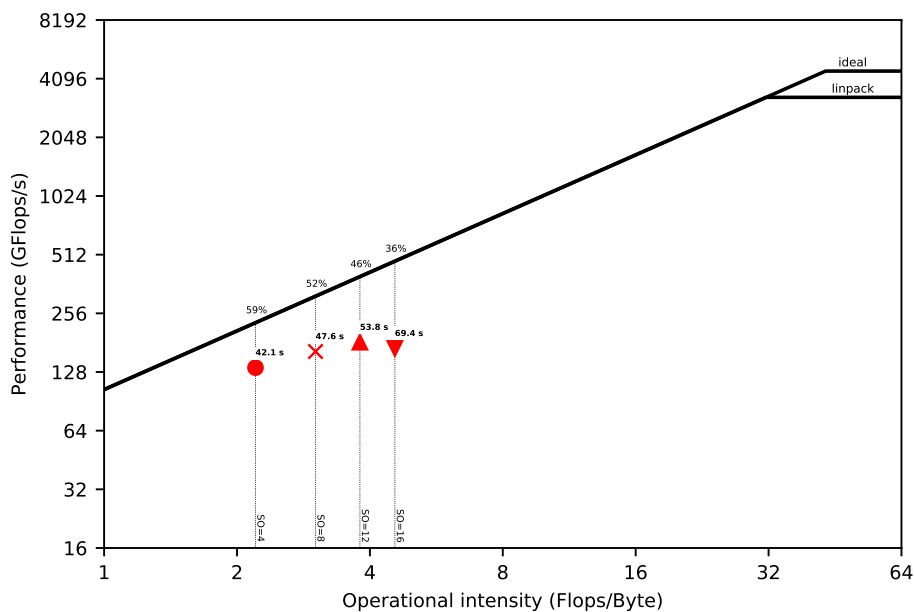
Figure 17. Roofline plots for a $768 \times 768 \times 768$ model on a Skylake 8180 architecture. The run times correspond to 1000ms of modeling for four different spatial discretization orders (4, 8, 12, 16).
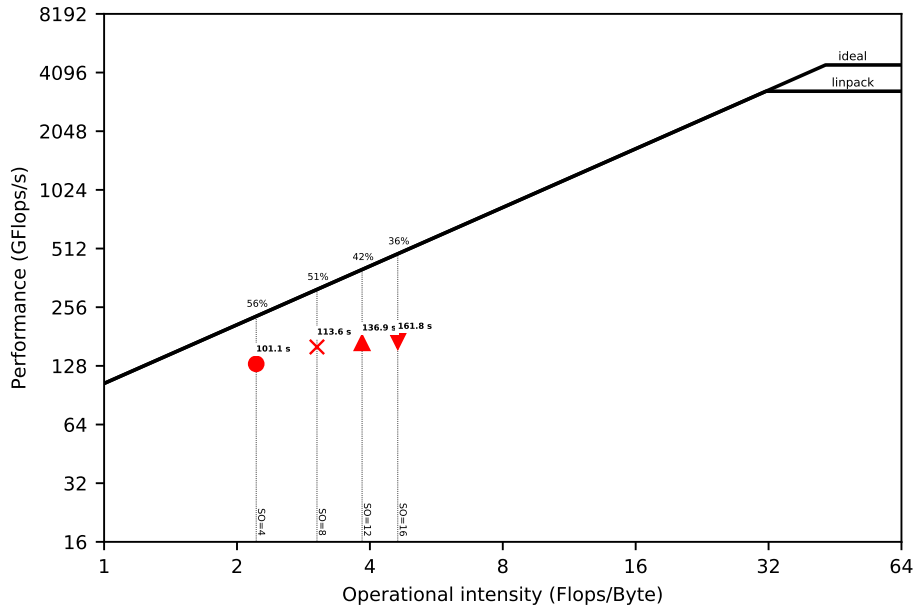
Figure 18. Roofline plots for a $1024 \times 1024 \times 1024$ model on a Skylake 8180 architecture. The run times correspond to 1000ms of modeling for four different spatial discretization orders (4, 8, 12, 16).

regime and the working sets never fit in the L3 cache. We also note a drop in performance with a 16th order discretization (relative to both the other space orders and the attainable peak), especially when using larger domains (Fig. 17 and 18). Our hypothesis, supported by profiling with Intel VTune (Intel Corporation, 2016), is that this is due to inefficient memory usage, in particular misaligned data accesses. Our plan to improve the performance in this regime consists of resorting to a specialized

5   stencil optimizer such as YASK (see Section 7). These results show that we have a portable framework that achieves good performance on different architectures. There is small room for improvements, as the machine peak is still relatively distant, but 50-60% of the attainable peak is usually considered very good. Finally, we remark that testing on new architectures will only require extensions to the Devito compiler, if any, while the application code remains unchanged.

7 Future Work

A key motivation for developing an embedded DSL such as Devito is to enable quicker development, simpler maintenance, and better portability and performance of solvers. The other benefit of this approach is that HPC developer effort can be focused on developing the compiler technology that is reapplied to a wide range of problems. This software reuse is fundamental to keep

5 the pace of technological evolution. For example, one of the current projects in Devito regards the integration of YASK (Yount, 2015), a lower-level stencil optimizer conceived by Intel for Intel architectures. Adding specialized backends such as YASK – meaning that Devito can generate and compile YASK code, rather than pure C/C++ – is the key for long-term performance portability, one of the goals that we are pursuing.

8 Conclusions

10 We have introduced a DSL for time-domain simulation for inversion and its application to a seismic inverse problem based on the finite difference method. Using the Devito DSL a highly optimized and parallel finite difference solver can be implemented within just a few lines of Python code. Although the current application focuses on features required for seismic imaging applications, Devito can already be used in problems based on other equations; a series of CFD examples are included in the code repository.

15 The code traditionally used to solve such problems is highly complex. The primary reason for this is that the complexity introduced by the mathematics is interleaved with the complexity introduced by performance engineering of the code to make it useful for practical use. By introducing a separation of concerns, these aspects are decoupled and both simplified. Devito successfully achieves this decoupling while delivering good computational performance and maintaining generality, both of which shall continue to be improved in future versions.

20 9 Code Availability

The code source code, examples and test script are available on github at https://github.com/opesci/devito and contains a README for installation. A more detailed overview of the project, list of publication and documentation of the software generated with Sphinx is available at http://www.devitoproject.org/. To install Devito:

```
git clone -b 'v3.1.0' https://github.com/opesci/devito
cd devito
conda env create -f environment.yml
source activate devito
pip install -e .
```

Acknowledgements. The development of Devito was primarily supported through the Imperial College London Intel Parallel Computing Centre. We would also like to acknowledgement the support from the SINBAD II project and support of the member organizations of the SINBAD Consortium as well as EPSRC grants EP/M011054/1 and EP/L000407/1.

References

Alnæs, M. S., Logg, A., Ølgaard, K. B., Rognes, M. E., and Wells, G. N.: Unified Form Language: a domain-specific language for weak formulations of partial differential equations, ACM Transactions on Mathematical Software (TOMS), 40, 9, 2014.

Andreolli, C., Thierry, P., Borges, L., Skinner, G., and Yount, C.: Chapter 23 - Characterization and Optimization Methodology Applied to Stencil Computations, in: High Performance Parallelism Pearls, edited by Reinders, J. and Jeffers, J., pp. 377 – 396, Morgan Kaufmann, Boston, doi:http://dx.doi.org/10.1016/B978-0-12-802118-7.00023-6, http://www.sciencedirect.com/science/article/pii/B9780128021187000236, 2015.

Arbona, A., Miñano, B., Rigo, A., Bona, C., Palenzuela, C., Artigues, A., Bona-Casas, C., and Massó, J.: Simflowny 2: An upgraded platform for scientific modeling and simulation, arXiv preprint arXiv:1702.04715, 2017.

Asanovic, K., Bodik, R., Catanzaro, B. C., Gebis, J. J., Husbands, P., Keutzer, K., Patterson, D. A., Plishker, W. L., Shalf, J., Williams, S. W., et al.: The landscape of parallel computing research: A view from berkeley, Tech. rep., Technical Report UCB/EECS-2006-183, EECS Department, University of California, Berkeley, 2006.

Backus, J.: The history of Fortran I, II, and III, in: History of programming languages I, pp. 25–74, ACM, 1978.

Bondhugula, U., Hartono, A., Ramanujam, J., and Sadayappan, P.: A Practical Automatic Polyhedral Parallelizer and Locality Optimizer, in: Proceedings of the 2008 ACM SIGPLAN Conference on Programming Language Design and Implementation, PLDI '08, pp. 101–113, ACM, New York, NY, USA, doi:10.1145/1375581.1375595, http://doi.acm.org/10.1145/1375581.1375595, 2008.

Cárdenas, A. F. and Karplus, W. J.: PDEL—a language for partial differential equations, Communications of the ACM, 13, 184–191, 1970.

Cauchy, A.-L.: Méthode générale pour la résolution des systèmes d'équations simultanées, Compte Rendu des Séances de L'Académie des Sciences XXV, Série A, 536–538, 1847.

Christen, M., Schenk, O., and Burkhart, H.: PATUS: A Code Generation and Autotuning Framework for Parallel Iterative Stencil Computations on Modern Microarchitectures, in: Proceedings of the 2011 IEEE International Parallel & Distributed Processing Symposium, IPDPS '11, pp. 676–687, IEEE Computer Society, Washington, DC, USA, doi:10.1109/IPDPS.2011.70, http://dx.doi.org/10.1109/IPDPS.2011.70, 2011.

Clayton, R. and Engquist, B.: Absorbing boundary conditions for acoustic and elastic wave equations, Bulletin of the Seismological Society of America, 67, 1529–1540, http://bssa.geoscienceworld.org/content/67/6/1529, 1977.

Colella, P.: Defining Software Requirements for Scientific Computing, 2004.

Cook Jr, G. O.: ALPAL: A tool for the development of large-scale simulation codes, Tech. rep., Lawrence Livermore National Lab., CA (USA), 1988.

Dongarra, J.: The LINPACK Benchmark: An Explanation, in: Proceedings of the 1st International Conference on Supercomputing, pp. 456–474, Springer-Verlag, London, UK, UK, http://dl.acm.org/citation.cfm?id=647970.742568, 1988.

Farrell, P. E., Ham, D. A., Funke, S. W., and Rognes, M. E.: Automated Derivation of the Adjoint of High-Level Transient Finite Element Programs, SIAM Journal on Scientific Computing, 35, C369–C393, doi:10.1137/120873558, http://dx.doi.org/10.1137/120873558, 2013.

Fomel et. al, S.: Madagascar: open-source software project for multidimensional data analysis and reproducible computational experiments, doi:http://doi.org/10.5334/jors.ag, 2013.

Haber, E., Chung, M., and Herrmann, F. J.: An effective method for parameter estimation with PDE constraints with multiple right hand sides, SIAM Journal on Optimization, 22, http://dx.doi.org/10.1137/11081126X, 2012.

Hawick, K. A. and Playne, D. P.: Simulation Software Generation using a Domain-Specific Language for Partial Differential Field Equations, in: 11th International Conference on Software Engineering Research and Practice (SERP'13), CSTN-187, p. SER3829, WorldComp, Las Vegas, USA, 2013.

Henretty, T., Veras, R., Franchetti, F., Pouchet, L.-N., Ramanujam, J., and Sadayappan, P.: A Stencil Compiler for Short-vector SIMD
5   Architectures, in: Proceedings of the 27th International ACM Conference on International Conference on Supercomputing, ICS '13, pp. 13–24, ACM, New York, NY, USA, doi:10.1145/2464996.2467268, http://doi.acm.org/10.1145/2464996.2467268, 2013.

Hopper, G. M.: The education of a computer, in: Proceedings of the 1952 ACM national meeting (Pittsburgh), pp. 243–249, ACM, 1952.

Igel, H.: Computational Seismology: A Practical Introduction, Oxford University Press, 1. edn., https://global.oup.com/academic/product/computational-seismology-9780198717409?cc=de{&}lang=en{&}, 2016.

10 Intel Corporation: Intel VTune Performance Analyzer, https://software.intel.com/en-us/intel-vtune-amplifier-xe, 2016.

Iverson, K. E.: A Programming Language, John Wiley & Sons, Inc., New York, NY, USA, 1962.

Jacobs, C. T., Jammy, S. P., and Sandham, N. D.: OpenSBLI: A framework for the automated derivation and parallel execution of finite difference solvers on a range of computer architectures, CoRR, abs/1609.01277, http://arxiv.org/abs/1609.01277, 2016.

Jones, J. L.: A survey of automatic coding techniques for digital computers, Ph.D. thesis, Massachusetts Institute of Technology, 1954.

15 Köster, M., Leißa, R., Hack, S., Membarth, R., and Slusallek, P.: Platform-Specific Optimization and Mapping of Stencil Codes through Refinement, in: Proceedings of the 1st International Workshop on High-Performance Stencil Computations, pp. 1–6, 2014.

Kukreja, N., Hückelheim, J., Lange, M., Louboutin, M., Walther, A., Funke, S. W., and Gorman, G.: High-level python abstractions for optimal checkpointing in inversion problems, arXiv preprint arXiv:1802.02474, 2018.

Kumar, R., Wason, H., and Herrmann, F. J.: Source separation for simultaneous towed-streamer marine acquisition –- a compressed sens-
20 ing approach, Geophysics, 80, WD73–WD88, doi:10.1190/geo2015-0108.1, https://www.slim.eos.ubc.ca/Publications/Public/Journals/Geophysics/2015/kumar2015sss/kumar2015sss_revised.pdf, (Geophysics), 2015.

Lange, M., Kukreja, N., Luporini, F., Louboutin, M., Yount, C., Hückelheim, J., and Gorman, G. J.: Optimised finite difference computation from symbolic equations, in: Proceedings of the 15th Python in Science Conference, edited by Katy Huff, David Lippa, Dillon Niederhut, and Pacer, M., pp. 89 – 96, 2017.

25 Lions, J. L.: Optimal control of systems governed by partial differential equations, Springer-Verlag Berlin Heidelberg, 1st edn., 1971.

Liu, Y. and Fomel, S.: Seismic data interpolation beyond aliasing using regularized nonstationary autoregression, GEOPHYSICS, 76, V69–V77, doi:10.1190/geo2010-0231.1, https://doi.org/10.1190/geo2010-0231.1, 2011.

Logg, A., Mardal, K.-A., Wells, G. N., et al.: Automated Solution of Differential Equations by the Finite Element Method, Springer, doi:10.1007/978-3-642-23099-8, 2012.

30 Louboutin, M., Lange, M., Herrmann, F. J., Kukreja, N., and Gorman, G.: Performance prediction of finite-difference solvers for different computer architectures, Computers & Geosciences, 105, 148–157, doi:https://doi.org/10.1016/j.cageo.2017.04.014, 2017.

Luporini, F., Varbanescu, A. L., Rathgeber, F., Bercea, G.-T., Ramanujam, J., Ham, D. A., and Kelly, P. H. J.: Cross-Loop Optimization of Arithmetic Intensity for Finite Element Local Assembly, ACM Trans. Archit. Code Optim., 11, 57:1–57:25, doi:10.1145/2687415, http://doi.acm.org/10.1145/2687415, 2015.

35 Luporini, F., Lange, M., Louboutin, M., Kukreja, N., Hückelheim, J., Yount, C., Witte, P., Kelly, P. H. J., Gorman, G. J., and Herrmann, F. J.: Architecture and performance of Devito, a system for automated stencil computation, CoRR, abs/1807.03032, http://arxiv.org/abs/1807.03032, 2018.

McCalpin, J. D.: STREAM: Sustainable Memory Bandwidth in High Performance Computers, Tech. rep., University of Virginia, Charlottesville, Virginia, http://www.cs.virginia.edu/stream/, a continually updated technical report. http://www.cs.virginia.edu/stream/, 1991-2007.

McMechan, G. A.: MIGRATION BY EXTRAPOLATION OF TIME-DEPENDENT BOUNDARY VALUES, Geophysical Prospecting, 31,
5   413–420, doi:10.1111/j.1365-2478.1983.tb01060.x, http://dx.doi.org/10.1111/j.1365-2478.1983.tb01060.x, 1983.

Membarth, R., Hannig, F., Teich, J., and Köstler, H.: Towards domain-specific computing for stencil codes in HPC, in: High Performance Computing, Networking, Storage and Analysis (SCC), 2012 SC Companion:, pp. 1133–1138, IEEE, 2012.

Meurer, A., Smith, C. P., Paprocki, M., Čertík, O., Kirpichev, S. B., Rocklin, M., Kumar, A., Ivanov, S., Moore, J. K., Singh, S., Rathnayake, T., Vig, S., Granger, B. E., Muller, R. P., Bonazzi, F., Gupta, H., Vats, S., Johansson, F., Pedregosa, F., Curry, M. J., Terrel, A. R., Roučka,
10   v., Saboo, A., Fernando, I., Kulal, S., Cimrman, R., and Scopatz, A.: SymPy: symbolic computing in Python, PeerJ Computer Science, 3, e103, doi:10.7717/peerj-cs.103, https://doi.org/10.7717/peerj-cs.103, 2017.

Mittet, R.: Implementation of the Kirchhoff integral for elastic waves in staggered-grid modeling schemes, GEOPHYSICS, 59, 1894–1901, doi:10.1190/1.1443576, http://dx.doi.org/10.1190/1.1443576, 1994.

Naghizadeh, M. and Sacchi, M. D.: f-x adaptive seismic-trace interpolation, GEOPHYSICS, 74, V9–V16, doi:10.1190/1.3008547, https:
15   //doi.org/10.1190/1.3008547, 2009.

Osuna, C., Fuhrer, O., Gysi, T., and Bianco, M.: STELLA: A domain-specific language for stencil methods on structured grids, in: Poster Presentation at the Platform for Advanced Scientific Computing (PASC) Conference, Zurich, Switzerland, 2014.

Patterson, D. A. and Hennessy, J. L.: Computer Organization and Design: The Hardware/Software Interface, Morgan Kaufmann Publishers Inc., San Francisco, CA, USA, 3rd edn., 2007.

20 Peters, B. and Herrmann, F. J.: Constraints versus penalties for edge-preserving full-waveform inversion, The Leading Edge, 36, 94–100, doi:10.1190/tle36010094.1, https://www.slim.eos.ubc.ca/Publications/Public/Journals/TheLeadingEdge/2016/peters2016cvp/peters2016cvp.html, (The Leading Edge), 2017.

Plessix, R.-E.: A review of the adjoint-state method for computing the gradient of a functional with geophysical applications, Geophysical Journal International, 167, 495–503, doi:10.1111/j.1365-246X.2006.02978.x, http://dx.doi.org/10.1111/j.1365-246X.2006.02978.x, 2006.

25 Raknes, E. B. and Weibull, W.: Efficient 3D elastic full-waveform inversion using wavefield reconstruction methods, Geophysics, 81, R45–R55, doi:10.1190/geo2015-0185.1, http://geophysics.geoscienceworld.org/content/81/2/R45, 2016.

Rathgeber, F., Ham, D. A., Mitchell, L., Lange, M., Luporini, F., McRae, A. T. T., Bercea, G., Markall, G. R., and Kelly, P. H. J.: Firedrake: automating the finite element method by composing abstractions, CoRR, abs/1501.01809, http://arxiv.org/abs/1501.01809, 2015.

Schmidt, M., van den Berg, E., Friedlander, M. P., and Murphy, K.: Optimizing Costly Functions with Simple Constraints: A Limited-
30   Memory Projected Quasi-Newton Algorithm, in: Proceedings of The Twelfth International Conference on Artificial Intelligence and Statistics (AISTATS) 2009, edited by van Dyk, D. and Welling, M., vol. 5, pp. 456–463, Clearwater Beach, Florida, 2009.

Seongjai Kim, H. L.: High-order schemes for acoustic waveform simulation, Applied Numerical Mathematics, 57, 402–414, http://www.hl107.math.msstate.edu/pdfs/rein/HighANM_final.pdf, 2007.

Sun, D. and Symes, W. W.: IWAVE implementation of adjoint state method, Tech. rep., Tech. Rep. 10-06, Department
35   of Computational and Applied Mathematics, Rice University, Houston, Texas, USA, https://pdfs.semanticscholar.org/6c17/cfe41b76f6b745c435891ea6ba6f4e2c2dbf.pdf, 2010.

Symes, W. W.: Acoustic Staggered Grid Modeling in IWAVE, THE RICE INVERSION PROJECT, p. 141, http://www.trip.caam.rice.edu/reports/2014/book.pdf#page=145, 2015a.

Symes, W. W.: IWAVE structure and basic use cases, THE RICE INVERSION PROJECT, p. 85, http://www.trip.caam.rice.edu/reports/2014/book.pdf#page=89, 2015b.

Symes, W. W., Sun, D., and Enriquez, M.: From modelling to inversion: designing a well-adapted simulator, Geophysical Prospecting, 59, 814–833, doi:10.1111/j.1365-2478.2011.00977.x, http://dx.doi.org/10.1111/j.1365-2478.2011.00977.x, 2011.

5 Tang, Y., Chowdhury, R. A., Kuszmaul, B. C., Luk, C.-K., and Leiserson, C. E.: The pochoir stencil compiler, in: Proceedings of the twenty-third annual ACM symposium on Parallelism in algorithms and architectures, pp. 117–128, ACM, 2011.

Tarantola, A.: Inversion of seismic reflection data in the acoustic approximation, GEOPHYSICS, 49, 1259, doi:10.1190/1.1441754, +http://dx.doi.org/10.1190/1.1441754, 1984.

Umetani, Y.: DEQSOL A numerical Simulation Language for Vector/Parallel Processors, Proc. IFIP TC2/WG22, 1985, 5, 147–164, 1985.

10 Unat, D., Cai, X., and Baden, S. B.: Mint: realizing CUDA performance in 3D stencil methods with annotated C, in: Proceedings of the international conference on Supercomputing, pp. 214–224, ACM, 2011.

Van Engelen, R., Wolters, L., and Cats, G.: Ctadel: A generator of multi-platform high performance codes for pde-based scientific applications, in: Proceedings of the 10th international conference on Supercomputing, pp. 86–93, ACM, 1996.

van Leeuwen, T. and Herrmann, F. J.: A penalty method for PDE-constrained optimization in inverse problems, In-
15 verse Problems, 32, 015 007, https://www.slim.eos.ubc.ca/Publications/Public/Journals/InverseProblems/2015/vanleeuwen2015IPpmp/vanleeuwen2015IPpmp.pdf, (Inverse Problems), 2015.

Versteeg, R.: The Marmousi experience; velocity model determination on a synthetic complex data set, The Leading Edge, 13, 927–936, http://tle.geoscienceworld.org/content/13/9/927, 1994.

Virieux, J.: P-SV wave propagation in heterogeneous media: Velocity-stress finite-difference method, GEOPHYSICS, 51, 889–901,
20 doi:10.1190/1.1442147, https://doi.org/10.1190/1.1442147, 1986.

Virieux, J. and Operto, S.: An overview of full-waveform inversion in exploration geophysics, GEOPHYSICS, 74, WCC1–WCC26, doi:10.1190/1.3238367, http://library.seg.org/doi/abs/10.1190/1.3238367, 2009.

Wang, S., Nissen, A., and Kreiss, G.: Convergence of finite difference methods for the wave equation in two space dimensions, Computing Research Repository, https://arxiv.org/abs/1702.01383, 2017.

25 Warner, M. and Guasch, L.: Adaptive waveform inversion: Theory, pp. 1089–1093, doi:10.1190/segam2014-0371.1, https://library.seg.org/doi/abs/10.1190/segam2014-0371.1, 2014.

Wason, H., Oghenekohwo, F., and Herrmann, F. J.: Low-cost time-lapse seismic with distributed compressive sensing–-Part 2: impact on repeatability, Geophysics, 82, P15–P30, doi:10.1190/geo2016-0252.1, https://www.slim.eos.ubc.ca/Publications/Public/Journals/Geophysics/2017/wason2016GEOPctl/wason2016GEOPctl.html, (Geophysics), 2017.

30 Watanabe, K.: Green's Functions for Laplace and Wave Equations, pp. 33–76, Springer International Publishing, Cham, doi:10.1007/978-3-319-17455-6_2, https://doi.org/10.1007/978-3-319-17455-6_2, 2015.

Weiss, R. M. and Shragge, J.: Solving 3D anisotropic elastic wave equations on parallel GPU devices., Geophysics, 78, doi:http://dx.doi.org/10.1190/geo2012-0063.1, 2013.

Williams, S., Waterman, A., and Patterson, D.: The Roofline model offers insight on how to improve the performance of software and
35 hardware., communications of the acm, 52, 2009.

Witte, P. A., Louboutin, M., Kukreja, N., Luporini, F., , Lange, M., Gorman, G. J., and Herrmann, F. J.: A large-scale framework for symbolic implementations of seismic inversion algorithms in Julia, https://www.slim.eos.ubc.ca/Publications/Private/Submitted/2018/witte2018alf/witte2018alf.html, submitted to Geophysics on March 1, 2018., 2018.

Witte, P. A., Louboutin, M., Lange, M., Kukreja, N., Luporini, F., Gorman, G., and Herrmann, F. J.: A large-scale framework for symbolic implementations of seismic inversion algorithms in Julia, 2018.

Witte, P. A., Louboutin, M., Lensink, K., Lange, M., Kukreja, N., Luporini, F., Gorman, G., and Herrmann, F. J.: Full-Waveform Inversion - Part 3: optimization, https://www.slim.eos.ubc.ca/Publications/Private/Submitted/2018/witte2018fwip3/witte2018fwip3.html, submitted
5   to The Leading Edge on December 15, 2017., 2018.

Yount, C.: Vector Folding: Improving Stencil Performance via Multi-dimensional SIMD-vector Representation, in: 2015 IEEE 17th International Conference on High Performance Computing and Communications, 2015 IEEE 7th International Symposium on Cyberspace Safety and Security, and 2015 IEEE 12th International Conference on Embedded Software and Systems, pp. 865–870, doi:10.1109/HPCC-CSS-ICESS.2015.27, 2015.

10   Zhang, Y. and Mueller, F.: Auto-generation and Auto-tuning of 3D Stencil Codes on GPU Clusters, in: Proceedings of the Tenth International Symposium on Code Generation and Optimization, CGO '12, pp. 155–164, ACM, New York, NY, USA, doi:10.1145/2259016.2259037, http://doi.acm.org/10.1145/2259016.2259037, 2012.